

Radio Emission from Anisotropic Electron Distributions

Gregory D. FLEISHMAN

National Radio Astronomy Observatory, Charlottesville, VA 22903 USA

(Received 2004 December 31; accepted 2005 January 1)

Abstract

The effect of pitch-angle anisotropy of fast electrons on generation of nonthermal radio emission is studied. Incoherent gyrosynchrotron radiation is shown to depend strongly on the anisotropy. In particular, the spectral index of gyrosynchrotron radiation increases up to a factor of 3-4 compared with the isotropic case. The degree of polarization (X-mode) increases for loss-cone distributions, while decreases for beam-like distributions. Ample evidence of the pitch-angle anisotropy effect on (1) spatial distribution of the radio brightness, (2) spatially resolved light curves of the intensity and polarization, (3) spectral hardness of microwave bursts, is found by exploring observations performed with Nobeyama Radioheliograph and Owens Valley Solar Array. Above some threshold in the angular gradient, the electron cyclotron maser instability (coherent gyrosynchrotron emission) can develop, provided that standard gyrosynchrotron emission is accompanied by a lower-frequency intense coherent emission. The coherent emission is studied in detail for a realistic distribution of fast electrons over the energy and pitch-angle. In agreement with observations of narrowband radio spikes, it is found that (1) hard (power-law) distributions over energy are preferable to produce the coherent emission, (2) the threshold of the instability corresponds to quite an anisotropic electron distribution, thus, the pitch-angle anisotropy derived from the properties of the continuum gyrosynchrotron radiation will not necessarily give rise to coherent emission (either enhanced isotropization implied by quasilinear saturation of the instability).

Key words: acceleration of particles—instabilities—radiation mechanisms:non-thermal—Sun:flares—Sun:radio radiation

1. Introduction

Observations of solar radio bursts with Nobeyama Radioheliograph (NoRH) revealed unambiguously the presence of anisotropic pitch-angle distributions of fast electrons accelerated in flares and accumulated in the radio sources. In particular, the existence of the microwave loop-top brightness peak of optically thin gyrosynchrotron (GS) emission (Melnikov et al. 2001; Kundu et al. 2001) has been interpreted as tracer of a strong concentration of mildly relativistic electrons trapped and accumulated in the top of a flaring loop (Melnikov et al. 2002a), which is an evidence of the transverse anisotropy of radiating electrons. Then, Lee & Gary (2000) studied the evolution of the radio spectrum of 1993 Jun 3 flare observed with Owens Valley Solar Array (OVSA) and found important indication of the anisotropic injection of fast electrons into the radio source and their consequent isotropisation due to angular scattering. The importance of the pitch-angle anisotropy for the modern radio data interpretation has been widely discussed during this Nobeyama Symposium (Altyntsev 2005; Bastian 2005; Gary 2005; Melnikov 2005). This paper discusses the effect of the pitch-angle anisotropy on generation of GS radiation (both incoherent and coherent).

A detailed study (stimulated by the mentioned findings) of incoherent GS emission produced by anisotropic pitch-angle distributions of the loss-cone and beam-like types is given in recent papers (Fleishman & Melnikov 2003a;

Fleishman & Melnikov 2003b). Accordingly, we outline only briefly why the anisotropy has actually a strong effect on GS emission.

The effect of anisotropy on the optically thin emission is primarily related to the energy-dependent directivity of the GS radiation. Indeed, most of the synchrotron radiation by a single ultrarelativistic electron is emitted within a narrow cone

$$\vartheta \sim \gamma_e^{-1} = mc^2/E \quad (1)$$

along the particle velocity, where γ_e is the Lorentz-factor of the electron, m , E are the mass and energy of the electron, c is the speed of light, so $\vartheta \ll 1$ if $\gamma_e \gg 1$. On the other hand, for semirelativistic and mildly relativistic electrons responsible for the GS emission, the directivity is not quite as strong, so the anisotropy (if present) can significantly change the radiation spectrum when the transition from moderately relativistic to highly relativistic regime occurs. Typical energies of fast electrons producing solar microwave continuum bursts (which are commonly believed to be produced by GS mechanism, e.g., Bastian et al. 1998) range from hundreds keV to a few MeV. Thus, the pitch-angle anisotropy of fast electrons in solar flares is particularly important for generation of microwave continuum radio emission, as well as for driving instabilities, which can result in coherent radio emissions.

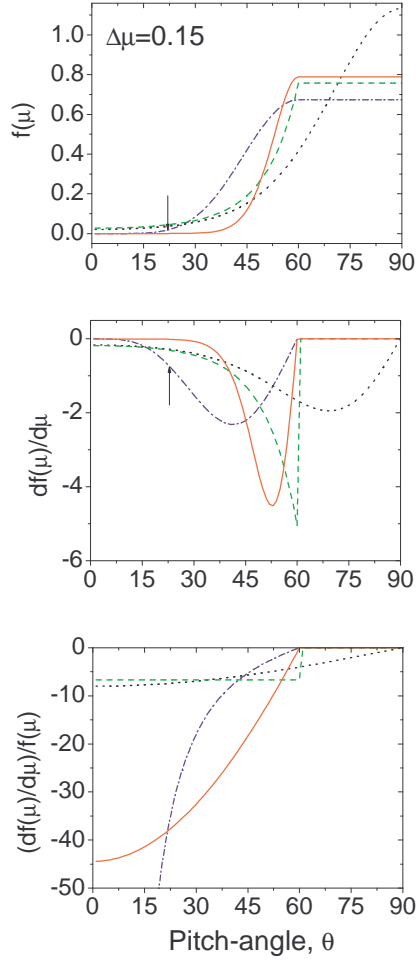


Fig. 1. Top: Angular distribution functions: gaussian (Fleishman & Yastrebov 1994a), dotted line; sin-N loss-cone (Aschwanden 1990) for $N = 6$, dash-dotted line; exponential loss-cone (5) for $\Delta\mu = 0.15$, dashed line; and gaussian loss-cone (6) for $\Delta\mu = 0.15$, solid line. The distributions are plotted for $\mu_0 = \cos\theta_c = 60^\circ$, all of them are normalized to unity. Middle: The derivatives of the angular distributions over μ . Bottom: the ratios of the derivatives to the distribution functions.

2. Angular Distribution Function

As a first approximation we consider a (simplified) factorized distribution function of fast electrons

$$f(\mathbf{p}) = \frac{N_e}{2\pi} f_1(p) f_2(\mu). \quad (2)$$

The distribution function (2) is normalized by d^3p

$$\int f(\mathbf{p}) p^2 dp d\mu d\varphi = N_e, \quad (3)$$

where N_e is the number density of fast electrons, $\mu = \cos\theta$, θ is the pitch-angle, φ is the azimuth angle, the specific distributions $f_1(p)$ and $f_2(p)$ are normalized as follows:

$$\int f_1(p) p^2 dp = 1, \quad \int_{-1}^1 f_2(\mu) d\mu = 1. \quad (4)$$

We assumed the distribution function over the momentum modulus to be a kind of power-law, while we consider a few different forms for the pitch-angle distribution to study the sensitivity of the GS properties to the shape of the angular distribution.

In addition to the gaussian and sin-N functions (explored by Fleishman & Melnikov 2003b), we use also the exponential loss-cone function

$$f_2(\mu) \propto \begin{cases} \exp\left(-\frac{\mu - \cos\theta_c}{\Delta\mu}\right), & \mu > \cos\theta_c, \\ 1, & -\cos\theta_c < \mu < \cos\theta_c \\ \exp\left(\frac{\mu + \cos\theta_c}{\Delta\mu}\right), & \mu < -\cos\theta_c, \end{cases} \quad (5)$$

and the gaussian loss-cone function

$$f_2(\mu) \propto \begin{cases} \exp\left(-\left(\frac{\mu - \cos\theta_c}{\Delta\mu}\right)^2\right), & \mu > \cos\theta_c, \\ 1, & -\cos\theta_c < \mu < \cos\theta_c \\ \exp\left(-\left(\frac{\mu + \cos\theta_c}{\Delta\mu}\right)^2\right), & \mu < -\cos\theta_c. \end{cases} \quad (6)$$

Let us consider these angular distributions (presented in figure 1) in more detail, having in mind that along with modification of incoherent GS emission the anisotropy can give rise to some instabilities (which depends on relative value of the angular gradient), in particular, to electron cyclotron maser (ECM) emission at the low gyroharmonics. The gaussian angular distribution provides rapid decrease of the number of electrons toward the direction of the magnetic field, and affect the GS substantially (Fleishman & Melnikov 2003b).

However, this distribution is not favorable to drive the instabilities (Fleishman & Yastrebov 1994a, 1994b), because the instability related to the gaussian angular distribution is rather weak being only slightly above the threshold. The efficiency of the instability is set up by relative importance of negative derivative of the distribution function over the momentum modulus and positive contribution related to angular gradient, which can be quantitatively described by the ratio of the angular gradient of the pitch-angle distribution to the angular distribution function itself. Although the angular derivative in figure 1 is not small, the peak value occurs at those angles where the angular distribution function is large, the ratio of these values is, therefore, small everywhere, figure 1 bottom. Thus, the gaussian pitch-angle distribution can be stable against instabilities for rather broad range of parameters.

Sin-N angular distribution (Aschwanden 1990) has very different properties. While this function looks rather smooth (it is continuous function together with its first derivative) and, thus, attractive for the use in theoretical calculations, it cannot be considered as a good approximation for the angular distribution since this function has a very deep intrinsic problem. Indeed, if we compare the behavior of the function and its first derivative, we discover that the derivative decreases (with the decrease of the pitch-angle) much more slowly than the function itself. Particularly, the arrows in figure 1 indicate the region where the derivative is of order of unity, while the

function is much less than unity. Note, that the ratio diverges as the pitch-angle decreases. Thus, $\sin-N$ function describes the case of highly unstable electron distribution, which gives rise to ECM instability operating significantly above the respective threshold for any parameters of this function. As a result, the instability exists for almost any shape of the momentum distribution of fast electrons, and its efficiency has extremely weak dependence on the electron spectral index. Such highly unstable distribution function can hardly be built up under reasonable assumptions about fast electron acceleration and transport.

This artificial property has already produced a few unexpected and poorly understood results. In particular, the detailed numerical calculations of the ECM quasilinear saturation (Aschwanden 1990) did not ensure the entire maser saturation even after 50 growth times: the peak value of the growth rate was reduced by less than one order of magnitude for this time. The reason for this surprising behavior is rather slow angular diffusion in the range of small pitch-angles, where the distribution function is small but the angular gradient is sufficiently large to provide the instability and then support it for quite a long time. The quasilinear relaxation occurs differently if the instability operates closer to its threshold (Fleishman & Arzner 2000).

Exponential loss-cone function (5) is free from such kind of problem. From the theoretical point of view it has only one disadvantage – discontinuity of its first derivative at $\theta = \theta_c$. Alternatively, a similar loss-cone distribution but with faster, gaussian, decrease of the number of electrons in the loss-cone (6) is also attractive from the theoretical point of view, since it is a function continuous together with its first derivative.

3. Incoherent Gyrosynchrotron Emission

The study of the GS emission produced by anisotropic pitch-angle distributions requires exact calculation of the corresponding emission and absorption coefficients (Fleishman & Melnikov 2003b). This is especially important for the directions along which a relatively small amount of particles is moving, so adding up the contributions from numerous electrons moving at unfavorable directions should be done correctly. Figure 2 presents an example of intensity, degree of polarization and spectral index of GS radiation produced by a gaussian angular distribution vs frequency as the degree of the anisotropy (angular gradient) changes (Fleishman & Melnikov 2003b).

The effect of the anisotropy on the properties of GS emission depends evidently on the viewing angle between the directions of wave propagation and the magnetic field. For the quasitransverse (QT) case, $\eta = 0.2$ ($\vartheta = 78^\circ$), right column, the effect of the pitch-angle anisotropy on the spectral index (bottom panel) is rather weak, while the intensity and degree of polarization increase with anisotropy increases. However, the anisotropy has exceedingly large effect on GS radiation produced at a quasisparallel (QP) direction, $\eta = 0.8$ ($\vartheta = 37^\circ$), left column. Indeed, the radiation intensity changes by orders of mag-

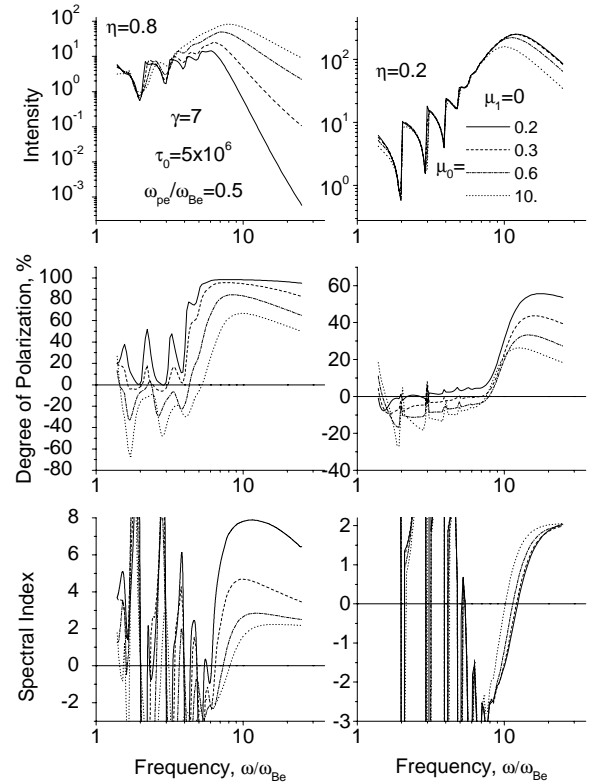


Fig. 2. GS radiation intensity, degree of polarization, and spectral index vs. frequency for various μ_0 in the Gaussian pitch-angle distribution $f_2 \propto \exp[-(\mu - \mu_1)^2 / \mu_0^2]$ of the loss-cone type, $\mu_1 = 0$

nitude compared with the isotropic case. Respectively, the difference in the spectral index in the optically thin frequency range is up to a factor of four (left panel, bottom). Remarkable change of polarization occurs as well: the degree of polarization increases in the optically thin region and can approach 100% for sufficiently high anisotropy. Furthermore, the sense of polarization can correspond to X-mode in the optically thin region contrary to the isotropic case.

Complementary, figure 3 shows the intensity, degree of polarization, and spectral index of GS emission observed at four different viewing angles from the gaussian (6) and exponential (5) loss-cone distributions (all other conditions are the same). GS emission is evidently very sensitive to the type of the angular distribution of fast electrons. The difference between these two distributions are seen most prominently in the spectral index plots: although the spectral index can be as large as 6 for the gaussian loss-cone distribution, it does not exceed 3 for the exponential loss-cone distribution.

Thus, this high sensitivity of the results to the type of the angular distribution can, in principle, be used to obtain important constraints on the pitch-angle distributions present during solar flares. We emphasize, that along

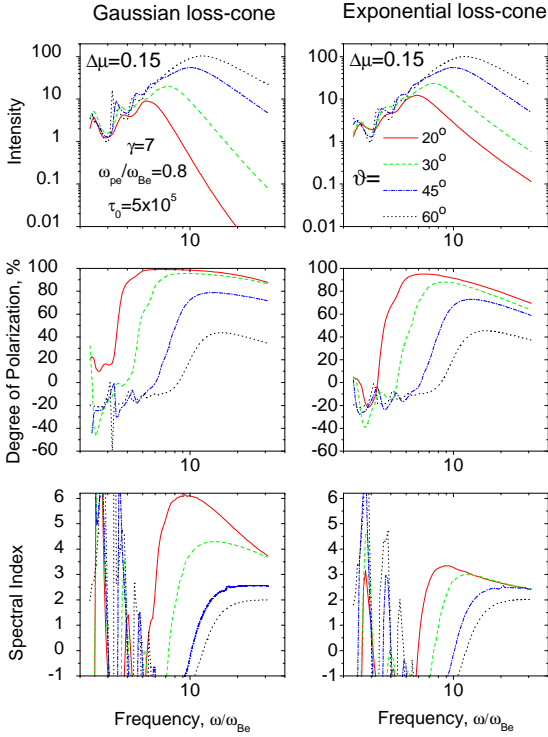


Fig. 3. GS radiation produced by fast electrons with a power-law distribution (with the index $\gamma = 7$) over momentum modulus and gaussian (6) (left) or exponential (5) (right) loss-cone functions. The total intensity, polarization and local spectral index are shown in the plot.

with strong effect on radiation intensity and spectral index, the anisotropy influences the degree of polarization, which also might be applied for quantitative diagnostics of the pitch-angle distribution.

Finally, we have to mention strong effect of pitch-angle anisotropy on the low-frequency "harmonic" structure of GS radiation (Fleishman & Melnikov 2003a). However, detection of this structure in the typical non-homogeneous sources requires high-resolution imaging spectroscopy, which is unavailable yet.

4. Anisotropy Build up in the Magnetic Loops

The importance of transport effects (Kennel & Petscheck 1966; Melrose & Brown 1976) for generation of nonthermal emissions during solar flares has been recognized long ago, in particular, the magnetic mirroring was argued to be a key process to account for the loop-top brightness peak of the optically thin GS emission (Melnikov et al. 2002a). This finding implies that the anisotropy can actually be built up due to transport effects even if the injection of fast electrons occurs isotropically (although this does not deny the possibility of anisotropic injection of fast electrons).

Typical treatment of the electron trapping at the magnetic loops frequently explores the idea of empty loss-cone due to particle precipitation and losses at the dense foot-points in the weak diffusion limit. Although this idea

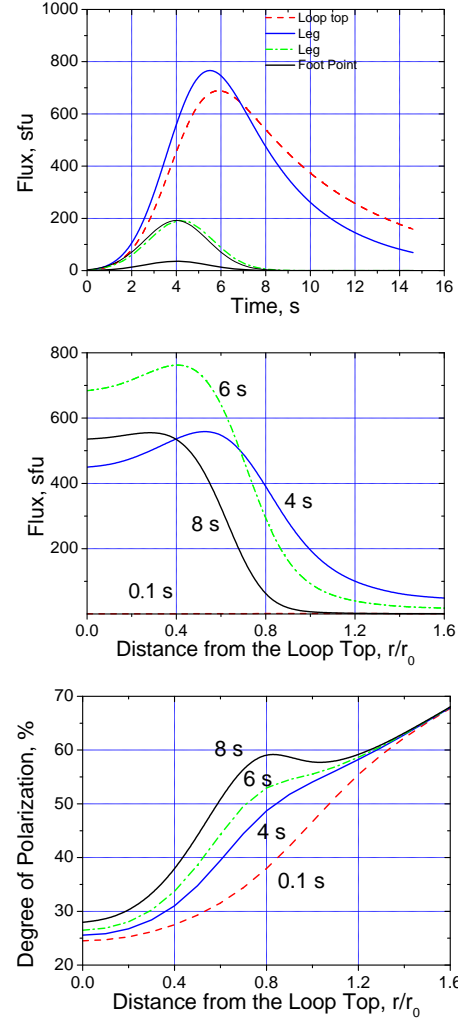


Fig. 4. Example of light curves of the microwave emission from a few positions along the loop for the case of isotropic injection function and angular-dependent life-time of fast electrons (top). The thin line represents the injection profile. Corresponding distributions (at a few time frames) of radio brightness (middle) and degree of polarization (bottom) along the magnetic trap.

brings an apparent advantage of the simplicity, it has also an important disadvantage of the discontinuity of the distribution function over the pitch-angle resulting in steep angular gradient, which affects strongly the calculation of the absorption coefficients.

To avoid the problems with the discontinuity and account for magnetic mirroring, energy losses and weak angular diffusion, we put forward a new model solution of the transport equation:

$$f(E, \mu, s, t) = \int_{-\infty}^t \exp\left(-\frac{t-t'}{\tau(E, \mu, s)}\right) g(E, \mu, s, t') dt' \quad (7)$$

where $g(E, \mu, s, t')$ and $f(E, \mu, s, t)$ are the injection and distribution functions of the fast electrons at the radio source vs energy E , the cosine of pitch angle μ , position along the loop s , and time t . Here the phenomenological life-time parameter τ can depend on the energy, position,

and *pitch-angle*.

For the weak diffusion regime we adopt that the life time τ display more or less fast decrease inside the loss-cone (when μ approaches the unity). This ensures smooth behavior of the distribution function, although the angular gradients can still be large for a favorable combination of parameters, and the net anisotropy can grow with time. Examples of the model radio brightness distributions at the subsequent times as a radio burst develops, and the spatially resolved light curves (at an optically thin frequency) in the context of anisotropic transport are shown in figure 4. To reveal the net effect of the angular-dependent transport, figure 4 assumes the life time of the electrons to depend on the pitch-angle of the electron only. It might be noted that the radio brightness peak moves towards the loop-top as the burst develops in agreement with observations (Melnikov et al. 2002a). Complementary, the emission from different locations along the loop displays systematic delay increasing from the foot-points to the loop-top, which has also been widely observed with NoRH data (Melnikov et al. 2002b; Melnikov 2005; Bastian 2005).

The dependence of the degree of polarization on time and its spatial distribution are highly affected by the pitch-angle anisotropy. Indeed, with isotropic injection, magnetic mirroring, and weak angular diffusion adopted in figure 4, the anisotropy increases with time progressively, which gives rise to the increase of the degree of polarization with time in the legs and top of the loop. At the foot-points ($r/r_0 > 1.4$), however, the angular distribution repeats the injected distribution since the life time of the electrons at the foot-points is too small to build up noticeable pitch-angle anisotropy.

5. Observational Evidence of Anisotropic Pitch-Angle Distribution in Flares

Besides already discussed spatial distributions of the radio brightness and spatially localized light curves, behavior of the degree of polarization typical for anisotropic pitch-angle distributions is frequently observed with NoRH. An example of the localized light curve (from one pixel of the magnetic loop leg) and corresponding time profile of the degree of polarization for the flare observed on 28-May-1993 is shown in figure 5. Remarkably, the absolute value of the degree of polarization keeps growing during the main peak of the burst, which is indicative for the increase of the anisotropy probably due to particle losses through the loss-cone, since other parameters affecting the polarization (magnetic field and the viewing angle) cannot change much at the localized region of the loop. The increase of the degree of polarization is followed by its decrease at a later stage of the burst. Interestingly, this turning point in the degree of polarization plot occurs at the same time as the break in the light curve where rapid decay of the radiation intensity slows down noticeably. This indicates that the losses due to precipitation into the loss-cone (which provides the anisotropisation of the electron distribution) are giving way to another decay

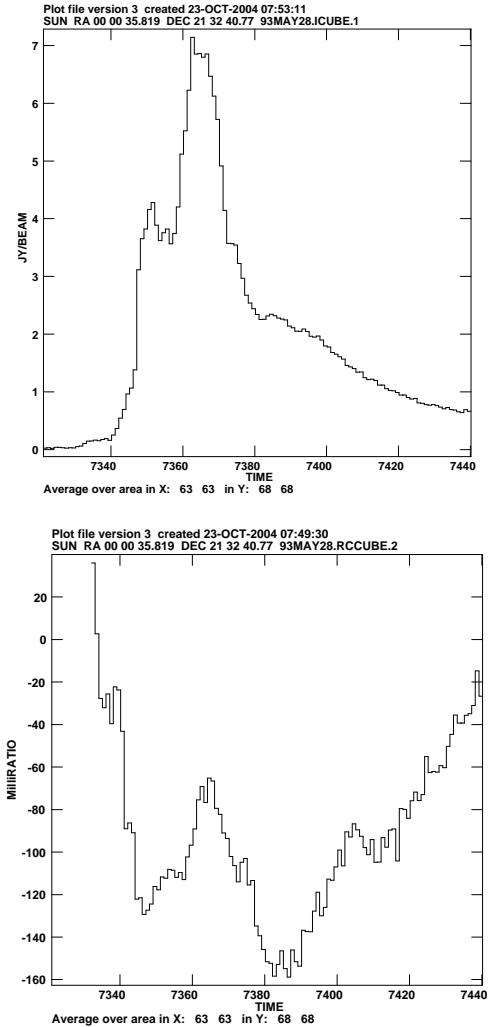


Fig. 5. A localized light curve (top) and and degree of polarization (bottom) for the 28-May-1993 event as observed at 17 GHz with NoRH (courtesy by T.S.Bastian).

process, probably, to Coulomb losses of already accumulated fast electrons. The Coulomb losses result it harder electron spectra, which generate GS radiation with weaker polarization.

A prominent spectral signature of the pitch-angle anisotropy has been found from the detailed analysis of two-component radio bursts composed of a high-frequency GS component and lower-frequency coherent component (Fleishman et al. 2003) observed with OVSA. Indeed, the microwave sources (accompanying the coherent dm spiky emission) observed at QP viewing angles to the magnetic field, figure 6, displays remarkably softer spectra at the optically thin region, than all other events on average, which can only be understood within the effect of loss-cone angular anisotropy on the GS spectrum. Moreover, all of the microwave bursts were highly polarized in the optically thin range (Fleishman et al. 2003), which is most probably related to the pitch-angle anisotropy of the loss-cone type (see figures 2, 3).

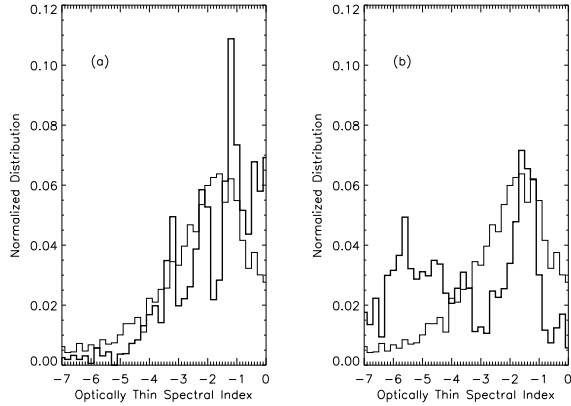


Fig. 6. The histograms of the high-frequency microwave spectral indices (Fleishman et al. 2003) for all bursts recorded by OVSA during 2001 (thin line), superimposed on the corresponding histogram for spike-producing microwave bursts observed at QT viewing angle (left) and QP viewing angle (right), thick lines. Strong excess of the steep spectra is observed in the QP case.

The difference in the spectral indices for these two classes of spike-producing microwave bursts (QT and QP) is as high as 3-4, which implies some important constraints on the shape of the angular distribution function. For example, the exponential decrease of the number of electrons in the loss-cone (5) turns to be too slow to provide the observed difference of 3-4 in spectral indices of optically thin GS emission at QP and QT directions (figure 3, right column). However, the gaussian loss-cone distribution (6) can evidently provide the required difference in the optically thin spectral indices (figure 3, left column). One can also note, that the gaussian loss-cone distribution provides stronger degree of polarization in the optically thin range than the exponential loss-cone distribution.

6. Electron Cyclotron Maser Emission

It is clear and has been well-known for a long time, that the pitch-angle anisotropy can drive instabilities, in particular, ECM instability. In essence, ECM emission is a coherent GS emission arising around lowest harmonics of the gyrofrequency when the absorption coefficient changes the sign and turns to be the amplification coefficient.

The theory of ECM emission in the solar corona has been extensively developed for the recent years (see Fleishman (2004a) for more detailed discussion and references). Big efforts have been made to consider the linear stage of the instability to specify the fastest growing wave-mode as a function of the plasma parameter $Y = \omega_{pe}/\omega_{Be}$, where ω_{pe} is the electron plasma frequency and ω_{Be} is the electron gyrofrequency.

Then, a particular attention has been paid to the role of absorption by the background coronal plasma in either emission source or along the ray path (in the harmonic gyrolayers) (Sharma et al. 1982; Sharma & Vlahos 1984). The absorption in gyrolayers was found to represent a se-

vere problem for the ECM emission to escape the corona (Sharma & Vlahos 1984), since the optical depth of the second gyrolayer calculated with the maxwellian background distribution is typically much larger than unity. However, estimates of nonlinear absorption (when the background distribution is modified by the incident powerful radiation) (Huang 1987) and particle-in-cell simulations (McKeen et al. 1990) show that even fundamental ECM emission has a chance to escape. Nevertheless, it remains unclear if the nonlinear absorption actually happens in solar conditions or not (and, accordingly, which harmonics can really escape the source to the observer).

Nonlinear stage of the ECM instability has also been studied. *One-dimensional* particle-in-cell simulations (Pritchett 1986) were found to agree well with a simplified analytical approach (Wu et al. 1981). The one-dimensional quasilinear saturation of the instability gives rise to a plateau formation in the distribution function of fast electrons over the transverse (to the magnetic field) velocity, providing, therefore, an absolute stabilization of the electron distribution. This means, that only the wave-mode with the largest growth rate can be amplified substantially, while weaker growing wave-modes remain practically unamplified.

The quasilinear relaxation is well known to occur rather differently for the *two-dimensional* case (Akhiezer et al. 1974) relevant to the ECM emission. Indeed, the relaxation due to the dominant mode affects the electron distribution in such a way that the new (modified) distribution is stable against this particular wave-mode. However, this new state is not necessarily stable against generation of other wave-modes, i.e., it is not absolutely stable distribution. Thus, other wave-modes can well continue to grow until they start to affect the electron distribution in their turn.

Two-dimensional fully relativistic numerical calculations of the ECM quasilinear relaxation (Aschwanden 1990) revealed many important properties of the relaxation process against the fastest growing mode. However, the initial sin-N distribution function adopted for the calculations has artificially large angular gradient in the range of pitch-angles practically free from fast electrons as has been already discussed in figure 1. Quasilinear relaxation has further been studied numerically for a particular set of the involved parameters when the lower-hybrid wave-mode has the largest growth rate (Fleishman & Arzner 2000). The electron distribution was shown to remain clearly anisotropic after the relaxation against the lower-hybrid waves. The new anisotropic distribution is, however, stable against the lower-hybrid waves, although unstable against the electromagnetic wave-modes in agreement with the general results of the plasma physics (Akhiezer et al. 1974). In addition, the time profile of the generated wave energy density was found to resemble the observed spike time profiles (Güdel & Benz 1990). Nevertheless, the ECM saturation process has not been studied in detail yet, thus, additional studies of the quasilinear relaxation against electromagnetic wave-modes are necessary.

The role of coronal inhomogeneities both in ECM source and at the ray path was analyzed. Effect of MHD-waves on the longitudinal transparency window (Robinson 1991a) and on the efficiency of the mode conversion (Robinson 1991b) was studied. Then, ECM line formation in a source with random inhomogeneities was found to produce either spectral broadening or splitting of the initial peak depending on the strength of the inhomogeneity (Fleishman 2004b). Mutual action of regular coronal non-uniformity and random local inhomogeneities was considered for a beam-like electron distributions (Vlasov et al. 2002).

In the previous section we concluded that the gaussian loss-cone function (6) is a good candidate for the electron pitch-angle distribution in the main source of continuum GS emission in the spike-producing events. Let us consider here the main properties of ECM emission produced by fast electrons with this angular distribution and power-law distribution over momentum modulus to be compared with the observed properties of the radio spikes appeared at the main phase of the burst. The results presented below are obtained numerically from fully relativistic calculations of the exact expressions of the GS absorption coefficient.

6.1. Basic parameters.

The growth rate value depends on many parameters, therefore, we first selected a set of basic parameters and then varied each of them successively. This approach allows to discuss properly what effect is produced by each particular parameter.

For our calculations we selected two basic values of the plasma frequency to gyrofrequency ratio, $Y = \omega_{pe}/\omega_{Be} = 1, 1.3$. When $Y = 1$, the most rapid growth of the extraordinary waves occurs at the second harmonics, $s = \omega/\omega_{Be} \approx 2$ and of the ordinary waves at the fundamental, $s \approx 1$, while for $Y = 1.3$ the growth of O1 waves becomes ineffective, and it is giving way to O2 waves.

The angular distribution (6) depends on two parameters: loss-cone angle θ_c and the width of the distribution $\Delta\mu$. We selected $\theta_c = 60^\circ$ and $\Delta\mu = 0.15$. The later value allows the instability to operate in the moderately-above-threshold regime. For the basic distribution of fast electrons over momentum we selected the following parameters typical for flares: $p_0/mc = 0.2$ ($E_{kin} \approx 10$ keV), $p_{br}/mc = 3$ ($E_{kin} \approx 1.1$ MeV) and $\gamma = 6$. It is assumed that at $p > p_{br}$ the power-law distribution is giving way to exponential cut-off.

6.2. Effect of plasma density.

The effect of plasma density on the growth rates at the lowest harmonics of the gyrofrequency was repeatedly studied for various electron distributions (Sharma et al. 1982; Sharma & Vlahos 1984; Li 1986; Winglee & Dulk 1986; Aschwanden 1990; Fleishman & Yastrebov 1994a; Fleishman & Yastrebov 1994b; Ledenev 1998; Stupp 2000; Fleishman 2004a). It has been established that for small $Y < 0.2 - 0.4$ the fundamental extraordinary waves (X1) have the largest growth rates. Then, for larger

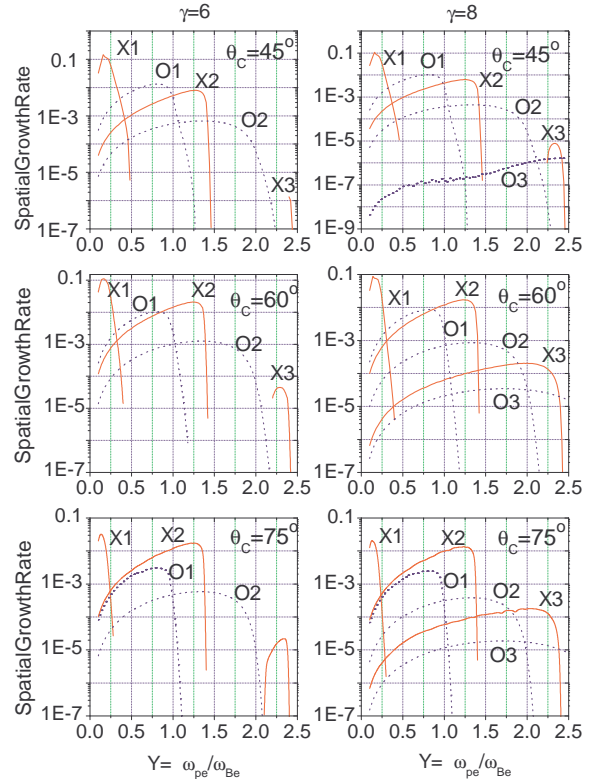


Fig. 7. Dimensionless spatial growth rates (normalized by $\frac{\pi\omega_{Be}}{2c} \frac{N_e}{N}$) for three first harmonics of the gyrofrequency for various parameters: $\gamma = 6$ (left column), $\gamma = 8$ (right column); $\theta_c = 45^\circ$ (top), $\theta_c = 60^\circ$ (middle), $\theta_c = 75^\circ$ (bottom). Set of basic parameters is used: $\Delta\mu = 0.15$, $p_0/mc = 0.2$, $p_{br}/mc = 3$.

Y , the amplification of X1 waves becomes inefficient and other waves become dominant (O1, X2, ...). Our calculations agree well with this standard picture (since it is largely related to kinematic restrictions).

The dependence of the growth rates on Y (for the adopted power-law momentum distribution and gaussian loss-cone angular distribution) in the limits $0.1 < Y < 2.5$ is given in figure 7. The growth rate of each harmonics decreases rapidly when the cut-off frequency of corresponding wave-mode exceeds the respective multiple of gyrofrequency (i.e., when $Y > 1$ for O1 waves, $Y > \sqrt{2}$ for X2 waves, $Y > 2$ for O2 waves etc). The absolute peak of the growth rate at a particular harmonics of the extraordinary waves is noticeably larger than of ordinary waves at the same harmonics. The absolute peak value decreases as the harmonic number increases.

The range of Y variation where a wave-mode is the fastest growing mode depends on parameters of the fast electron distribution. In particular, for small loss-cone angle value (top), the growth rates of O1 waves are larger than of X2 waves for $Y < 1$. However, the difference between them decreases as θ_c increases (middle) and X2 waves grow faster than O1 waves for large θ_c (bottom) in agreement with the finding by Winglee & Dulk (1986). Respectively, O1 mode grows faster than X2 mode if $Y < 1$ for $\theta_c = 45^\circ$, if $Y < 0.85$ for $\theta_c = 60^\circ$, and never for $\theta_c = 75^\circ$.

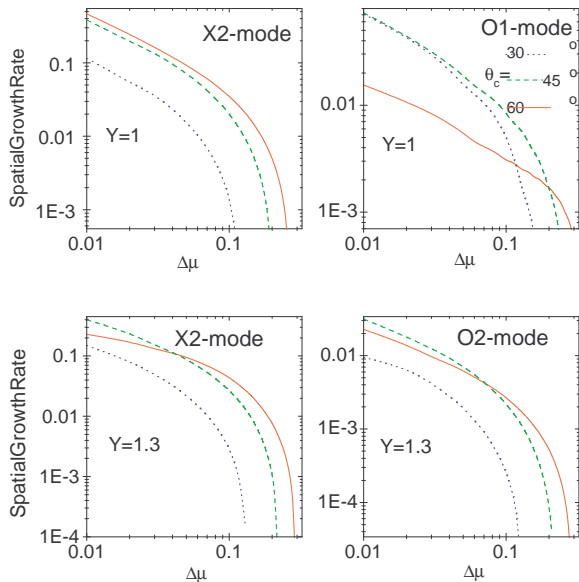


Fig. 8. Spatial growth rates for X2-, O1-, and O2- modes vs width of the loss-cone distribution $\Delta\mu$ for the basic set of parameters and three θ_c values.

Then, for $Y > \sqrt{2}$ the O2 mode is the dominant, and for $Y > 1.8$ the X3 mode may dominate (if it is unstable for a particular set of parameters).

We note an interesting feature specific for our electron distribution: the amplification of the third harmonics of both extraordinary and ordinary waves is ineffective for hard electron spectra (e.g., $\gamma = 6$, left column) for most of the Y range, while it is effective for softer spectra (e.g., $\gamma = 8$, right column). The reason for the instability suppression for the hard spectrum is the destructive contribution of (true absorption by) high-energy electrons. For softer electron distributions the role of high-energy electrons is less important allowing the instability at the third harmonics. Note that for the gaussian angular distribution used in (Fleishman & Yastrebov 1994a, 1994b), the instability suppression by high-energy tail of power-law distribution is important even at the fundamental and second harmonics, since the gaussian distribution provides weaker angular gradients than considered here gaussian loss-cone distribution (6).

6.3. Effect of angular distribution.

The dependences of the maximized (over the emission frequency and angle) spatial growth rates on θ_c displays bell-shaped curves for any mode. The most effective amplification of O1 waves occurs around $\theta_c \approx 45^\circ$, while around $\theta_c \approx 60^\circ$ for O2 waves and even higher values for X2 waves. No qualitative difference is seen for various electron spectral indices γ .

Of particular importance is the dependence on the width of the distribution $\Delta\mu$, figure 8. Evidently, all the growth rates increase as $\Delta\mu$ decreases because this corresponds to stronger angular gradients, and, thus, to stronger instability. However, the growth rates decrease as

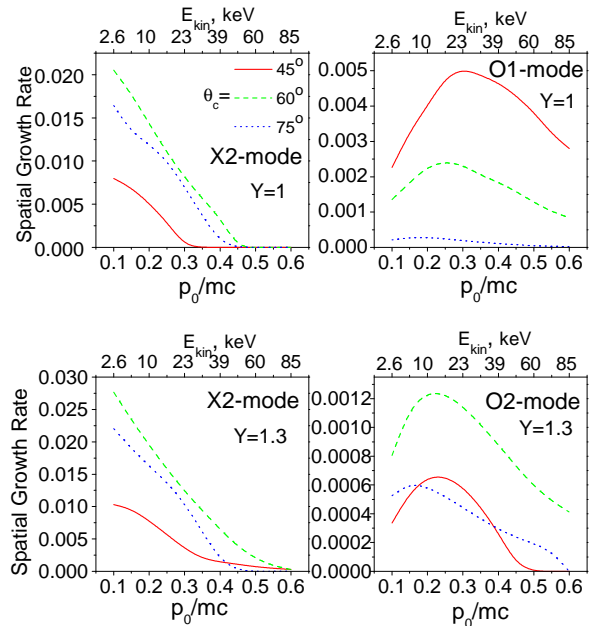


Fig. 9. Spatial growth rates for X2-, O1-, and O2- modes vs minimal momentum of fast electrons p_0 for the basic set of parameters and three θ_c values.

$\Delta\mu$ increases first gradually and then rapidly. This rapid decrease occurs when the instability approaches its threshold provided by negative contribution of the momentum term ($\partial f/\partial p = -\gamma f$) in the expression for the GS absorption coefficient. When $\Delta\mu$ exceeds 0.1–0.3 (depending on other parameters) the instability disappears. We emphasize that this happens when the pitch-angle distribution of fast electrons remains clearly anisotropic. Thus, such anisotropic distributions can generate standard GS emission without coherent ECM emission.

The detailed shape of the curves depends on other parameters, like Y and θ_c . For X2 and O2 waves, large θ_c values are preferable, while for O1 waves – lower θ_c values. However, for all considered cases, $\theta_c = 60^\circ$ has the largest threshold $\Delta\mu$ value.

6.4. Effect of distribution over momentum.

The growth rates of all considered wave-modes display rather weak dependence on p_{br} for the selected set of basic parameters, so we do not present the corresponding plots. We should note, however, that this property of the ECM emission is model-dependent and valid if the instability operates noticeably above the threshold. If the instability is very close to its threshold, the behavior of the momentum distribution in the high-energy range may be important. In particular, this is the case of gaussian pitch-angle distribution (Fleishman & Yastrebov 1994a, 1994b).

The dependence of the growth rates on the minimal momentum p_0 is shown in figure 9. Shape of the curves is clearly different for various harmonics and wave-modes. X2 waves display decreasing curves with increasing p_0 ,

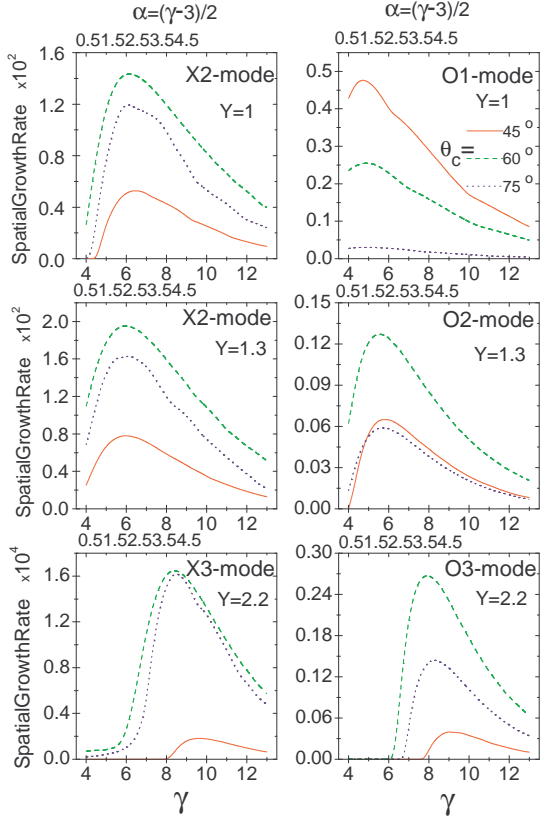


Fig. 10. Spatial growth rates for X2-, X3-, O1-, O2-, and O3- modes vs spectral index of fast electron distribution γ for the basic set of parameters and three θ_c values.

thus, low-energy electrons are preferable to produce these waves. Wide loss-cones ($\theta_c = 60^\circ$, 75°) provide larger growth rates than narrower loss-cone ($\theta_c = 45^\circ$).

Ordinary waves are generated most effectively if the low-energy cut-off is about 20 keV for O2-mode and about 10 keV for O1 mode, although the corresponding peaks are rather broad. Narrow loss-cone ($\theta_c = 45^\circ$) is the most efficient to produce O1 waves and wider one ($\theta_c = 60^\circ$) is preferable to produce O2 waves. The wide loss-cone of $\theta_c = 75^\circ$ is less effective for the both harmonics of the ordinary waves.

Considering together the plots in figure 9, we can conclude that different fractions of fast electrons are responsible for generation of these different wave-modes. Thus, quasilinear relaxation against one (the dominant) mode should not necessarily provide saturation of all other wave-modes in agreement with numerical quasilinear simulations (Fleishman & Arzner 2000).

The dependences of the growth rates on the electron spectral index γ are of particular importance, since they can be compared with observations of accompanying continuum (microwave and HXR) emissions. All the curves shown in figure 10 are bell-shaped; peak of each curve corresponds to a favorable γ value specific for each wave-mode. The decrease of the growth rates for harder spectra (smaller γ) is provided by negative contribution of

high-energy electrons at large harmonics. The decrease for softer spectra (larger γ) is related to the increase of the instability threshold that is proportional to γ for the power-law momentum distribution of the electrons.

The favorable γ value depends on the harmonic number and type of the wave. X2 waves have the peak around $\gamma = 6$ (which corresponds to the synchrotron spectrum with the index 1.5) for a broad range of the involved parameters. A bit lower values are favorable for O2 waves. However, O1 waves display the peak at rather small values $\gamma = 4 - 5$.

It is remarkable that the favorable γ values for the third harmonics are significantly larger than for the fundamental and second harmonics: it is about 8 (synchrotron spectral index 2.5) for O3 waves and even larger for X3 waves. Such a different behavior of the curves for the different waves can in principle be used to specify the contribution of various harmonics to the spike radiation.

7. Discussion

We conclude the pitch-angle anisotropy to affect significantly the radio emission from solar flares. First of all, we should mention the strong effect of the anisotropy on the intensity and spectral index of the emission in the optically thin region, which relates primarily to the energy-dependent directivity (1) of the synchrotron radiation by a single electron.

Currently, it is discovered with the NoRH data that microwave emission from the foot-point parts of extended flaring loops displays systematically softer spectra ($\Delta\alpha \sim 1-1.5$ in the domain 17 GHz to 34 GHz) than from the loop-top part (Yokoyama et al. 2002; Melnikov 2005). Evidently, the pitch-angle anisotropy can make an important contribution to the observed spectral index variations. Indeed, if we take into account the convergence of the magnetic field lines towards the foot-points, we should expect a more anisotropic electron distribution (due to a larger loss-cone) in the foot-point source than in the loop-top source. Furthermore, for the disc flares the foot-point source is observed at a QP direction, while the loop-top source is observed at a QT direction, which results in *systematically* softer spectra of GS radiation from the foot points compared with the loop-top. Thus, the pitch-angle anisotropy probably plays a key role in the observed variations of the spectral index of the microwave radiation along the loop. Moreover, the pitch-angle anisotropy has strong effect on polarization properties of GS emission, which is widely observed with NoRH.

Coherent GS emission (ECM) is also highly relevant for understanding the current radio observations. The available data about the radio spikes are pretty consistent with the idea that the source of spike cluster is a loop filled by fast electrons and relatively tenuous background plasma (Fleishman et al. 2003). The trapped fast electrons (with a power-law energy spectrum and a loss-cone angular distribution) produce continuum GS emission through the *entire* loop, while each single spike is generated in a *local* source inside this loop by ECM mechanism when some fa-

avorable conditions are fulfilled. Most probably, the local source is formed when the local anisotropy is increased compared with the averaged one to produce ECM emission (Fleishman & Melnikov 1998). The assumed fluctuations of the pitch-angle distribution of fast electrons can be produced by the magnetic turbulence (Fleishman & Melnikov 1998; Barta & Karlicky 2001). Accordingly, if the averaged angular distribution is stable against ECM generation, the number of spikes in an event should increase as the intensity of the magnetic turbulence increases (and other equal conditions). Complementary, the closer the averaged angular distribution to the instability threshold, the larger the amount of the local sources (and, respectively, the number of spikes) might be formed by the same magnetic turbulence.

The scale of a single spike source is estimated (indirectly) as ~ 200 km (Benz 1985); a wave should experience many e-folding amplifications over this length to produce observable spike with large brightness temperature, so this requirement reads $\kappa \gg 5 \cdot 10^{-8} \text{ cm}^{-1}$, where κ is the spatial amplification coefficient. We conclude (from the numbers in figure 7) that the required amplification can easily be provided for the fundamental and second harmonics of both X- and O- modes. Moreover, the amplification of X3 mode is also possible if fast particles are numerous enough, $N_e/N \gtrsim 10^{-2}$, while the amplification of O3 mode is less probable.

The dependence of the growth rate on the fast electron distribution is of primary importance since it can be compared with the observations. Indeed, the decrease of the growth rates with the γ increase corresponds to smaller efficiency of the ECM emission for softer spectra of fast electrons. The correlation of this type is actually observed when spectra of microwave or HXR emission simultaneous to spike bursts are analyzed: the harder the fast electron spectrum the stronger the averaged spike flux (Fleishman et al. 2003). The range of microwave spectral indices is typically $\alpha = 1 - 4$. Thus, we can conclude that most of the spikes are generated at a harmonics not larger than second. ECM emission at the third harmonics (see Figure 10) is the most efficient if $\gamma \approx 8$ ($\alpha \approx 2.5$), therefore, the softer microwave spectra should be preferable for the third harmonics generation in the range $\alpha < 2.5$, which has not been observed for spikes yet.

Then, the dependences on the angular gradient value ($\Delta\mu$) display clearly that the instability disappears (as $\Delta\mu$ increases) when the pitch-angle distribution still remains highly anisotropic ($\Delta\mu = 0.2 - 0.3$). Accordingly, the overall distribution of fast electrons accumulated at the loop may be rather anisotropic for a long time providing noticeably softer GS spectra (for a QP viewing angle) than the isotropic distribution, which is observed indeed (Fleishman et al. 2003).

The National Radio Astronomy Observatory is a facility of the National Science Foundation operated under cooperative agreement by Associated Universities, Inc. This work was supported in part by NSF grant AST-0307670 and NASA grant NAG5-11875 to New Jersey Institute of Technology, and by the RFBR grants No.03-02-17218, 04-02-39029.

References

- Akhiezer, A.I., Akhiezer, I.A., Polovin, R.V., Sitenko, A.G., & Stepanov, K.N. Plasma Electrodynamics, (Ed. - A.I.Akhiezer), Moscow, Nauka 1974 (Pergamon, Oxford, 1975)
- Altyntsev, A.T. 2005, Proc. of Nobeyama Symposium
- Aschwanden, M.J. 1990, A&AS, 85, 1141
- Aschwanden, M.J., & Güdel, M. 1992 ApJ, 401, 736
- Barta, M., & Karlicky, M. 2001, A&A, 379, 1045
- Bastian, T.S. 2005, Proc. of Nobeyama Symposium
- Bastian, T.S., Benz, A.O., & Gary, D.E. 1998, ARAA, 36, 131
- Benz, A.O. 1985, Sol. Phys., 96, 357
- Fleishman, G.D. 2004a, Astron. Zh., 81, 72 (transl.: Astron. Repts., 48, 65)
- Fleishman, G.D. 2004b, ApJ, 601, 559
- Fleishman, G.D., & Arzner, K. 2000, A&A, 358, 776
- Fleishman, G.D., Gary, D.E., & Nita, G.M. 2003, ApJ, 593, 571
- Fleishman, G.D., & Melnikov, V.F. 1998, Usp. Fiz. Nauk, 168, 1265 (transl.: Physics - Uspekhi, 41, 1157)
- Fleishman, G.D., & Melnikov, V.F. 2003a, ApJ, 584, 1071
- Fleishman, G.D., & Melnikov, V.F. 2003b, ApJ, 587, 823
- Fleishman, G.D., & Yastrebov, S.G. 1994a, Sol. Phys., 153, 389
- Fleishman, G.D., & Yastrebov, S.G. 1994b, Astron. Zhurn., 71, 531
- Gary, D.E. 2005, Proc. of Nobeyama Symposium
- Güdel, M., & Benz, A.O. 1990, A&A, 231, 202
- Huang, G.-L. 1987, Sol. Phys., 114, 363
- Kennel, C.F., & Petschek, H.E. 1966, J. Geophys. Res., 71, 1
- Kundu, M.R., Nindos, A., White, S.M., & Grechnev, V.V. 2001, ApJ, 557, 880
- Lee, J., & Gary, D.E. 2000, ApJ, 543, 457
- Ledenev, V.G. 1998, Sol. Phys., 179, 405
- Li, H.W. 1986, Sol. Phys., 104, 131
- McKeen, M.E., Winglee, R.R., & Dulk, G.A. 1990 in Proc. of 3th Workshop Max'91 Solar Flares (Eds. R.R.Winglee & A.L.Kiplinger), Colorado, Boulder, p.29
- Melnikov, V.F. 2005, Proc. of Nobeyama Symposium
- Melnikov, V.F., Shibasaki, K., Nakajima, H., Yokoyama, T. & Reznikova, V.E. 2001, CESRA Workshop (München, 2-6 July 2001)
- Melnikov, V.F., Shibasaki, K., & Reznikova, V.E. 2002a, ApJL, 580, L185
- Melnikov, V.F., Reznikova, V.E., Yokoyama, T., and Shibasaki, K. 2002b, in: Proc. of the SPM-10 "Solar Variability: From Core to Outer Frontiers", Prague (ESA SP-506, December 2002), ed. A.Wilson, p.p.339-342
- Melrose, D.B., & Brown, J.C. 1976, MNRAS, 176, 15
- Pritchett, P.L. 1986, Phys. Fluids, 29, 2919
- Robinson, P.A. 1991a, Sol. Phys., 134, 299
- Robinson, P.A. 1991b, Sol. Phys., 136, 343
- Sharma, R.R., & Vlahos, L. 1984, ApJ, 280, 405
- Sharma, R.R., Vlahos, L., & Papadopoulos, K. 1982, A&A, 112, 377
- Stupp, A. 2000, MNRAS, 311, 251
- Vlasov, V.G., Kuznetsov, A.A., & Altyntsev, A.T. 2002, A&A, 382, 361
- Winglee, R.R., & Dulk, G.A. 1986, Sol. Phys., 104, 93
- Wu, C.S, Tsai, S.T., Xu, M.J., & Shen, J.W. 1981, ApJ, 248, 384
- Yokoyama, T., Nakajima, H., Shibasaki, K., Melnikov, V.F., & Stepanov, A.V. 2002, ApJL, 576, L87